Time-frequency representations of Lamb waves

Marc Niethammer and Laurence J. Jacobs[a)]
School of Civil and Environmental Engineering, Georgia Institute of Technology, Atlanta, Georgia 30332-0355

Jianmin Qu and Jacek Jarzynski
G. W. Woodruff School of Mechanical Engineering, Georgia Institute of Technology, Atlanta, Georgia 30332-0405

(Received 26 July 2000; revised 20 December 2000; accepted 21 January 2001)

The objective of this study is to establish the effectiveness of four different time-frequency representations (TFRs)—the reassigned spectrogram, the reassigned scalogram, the smoothed Wigner–Ville distribution, and the Hilbert spectrum—by comparing their ability to resolve the dispersion relationships for Lamb waves generated and detected with optical techniques. This paper illustrates the utility of using TFRs to quantitatively resolve changes in the frequency content of these nonstationary signals, as a function of time. While each technique has certain strengths and weaknesses, the reassigned spectrogram appears to be the best choice to characterize multimode Lamb waves. © *2001 Acoustical Society of America.* [DOI: 10.1121/1.1357813]

PACS numbers: 43.20.Mv, 43.35.Cg [DEC]

I. INTRODUCTION

There have been significant advances in the field of signal processing since the development of the fast Fourier transform (FFT) in the mid 1960's. Current research is primarily concentrated on applications for microelectronics and telecommunications, although most signal-processing techniques are general enough in nature to have potential applications in a variety of fields. Recent work in the area of time-frequency representations (TFRs) such as the spectrogram, the scalogram, the Wigner–Ville distribution, and the Hilbert spectrum shows great promise for applications in nondestructive evaluation. Of particular interest (and importance) is the use of TFRs to interpret ultrasonic guided waves. This class of ultrasonic signals can be extremely complicated, exhibiting dispersion and containing multiple modes.

This paper compares the effectiveness of four candidate TFRs to characterize Lamb waves—guided ultrasonic waves that propagate in plates. Lamb waves have received extensive attention since the study by Mindlin.[1] Recent experimental work has shown that it is possible to obtain a plate's dispersion relationship by using the two-dimensional Fourier transform (2D-FT) to operate on multiple, equally spaced waveforms.[2,3] Unfortunately, the need for exact, spatially sampled data restricts the practicality of the 2D-FT for some inspection applications. In contrast, TFRs require only a single signal. Recently, Prosser *et al.*[4] used the smoothed Wigner–Ville distribution to determine the Lamb modes of numerically simulated waveforms in an aluminum plate. They also consider real experimental data for a composite plate and identify the s_0 and the a_0 Lamb modes for frequencies below 500 kHz. Hayashi *et al.*[5] determined the thickness and the elastic properties of thin metallic foils (thickness of less than 40 μm) by calculating the group velocity of a single mode (the a_0 up to 3.5 MHz) using the wavelet transform of laser-generated and -detected Lamb waves. Holland *et al.*[6] used a reassigned, smoothed Wigner–Ville distribution to examine synthetic waves in a 10-mm-thick steel plate with excellent results. Niethammer *et al.*[7] showed that the reassigned spectrogram is capable of distinguishing multiple, closely spaced Lamb modes in the ultrasonic frequency range.

The current study extends[7] by evaluating the suitability of the reassigned spectrogram, the reassigned scalogram, the smoothed Wigner–Ville distribution, and the Hilbert spectrum to extract the dispersion curves of a plate from a single time-domain signal. The objective of this paper is to establish the robustness of this collection of TFRs by comparing their ability to resolve the dispersion relationships for Lamb waves generated and detected with optical techniques (laser source and interferometric detector).

II. BRIEF REVIEW OF TFRs

A transient time-domain signal, together with its Fourier transformed spectrum, does not provide enough information for applications that require an understanding of how a signal's frequency changes *as a function of time*. Note that the Fourier transform is essentially limited to stationary signals—signals that have the same frequency content for all times. In contrast, nonstationary signals require signal-processing methods that can quantitatively resolve changes in frequency content, as a function of time. A large number of TFRs have been developed to analyze nonstationary signals, many of which are subsumed in the general framework of Cohen's class.[8]

This section provides a brief review of TFRs to furnish a common foundation and assist in understanding why certain TFRs are more effective in this application—it is not intended to be a comprehensive review, and references that contain technical details and mathematical derivations are provided for an interested reader.

[a)]Author to whom correspondence should be addressed. Electronic mail: laurence.jacobs@ce.gatech.edu

The short-time Fourier transform (STFT) divides a time-domain signal into a series of small overlapping pieces; each of these pieces is windowed and then individually Fourier transformed.[8] The STFT of a function $s(t)$ is defined as

$$S_1(\omega,t)=\frac{1}{2\pi}\int_{-\infty}^{\infty}e^{-i\omega\tau}s(\tau)h(\tau-t)\mathrm{d}\tau, \tag{1}$$

where $h(t)$ is a window function. The energy density spectrum of an STFT is defined as $E_1(\omega,t)=|S_1(\omega,t)|^2$ and called a spectrogram.

Instead of a fixed window function, the wavelet transform (WT) uses time-frequency atoms or wavelets. The WT of a function $s(t)$ is given by[9]

$$S_2(a,b)=\frac{1}{\sqrt{a}}\int_{-\infty}^{\infty}s(t)\psi\left(\frac{t-b}{a}\right)\mathrm{d}t, \tag{2}$$

where a is the scale, and b the time-shift variable (a and b are also known as the dilation and the translation parameters, respectively). A small a corresponds to a high frequency and vice versa [a dilates the mother wavelet $\psi(t)$, while b simply shifts the wavelet with respect to time without altering the frequency content]. The energy density function of a WT is defined as $E_2(a,b)=|S_2(a,b)|^2$ and is called a scalogram.

Wavelets are derived from a mother wavelet $\psi(t)$ by dilation and translation. This study uses the Gabor wavelet

$$\psi(t)=\frac{1}{\sqrt[4]{\pi}}\sqrt{\frac{\omega_0}{\gamma}}e^{-1/2(\omega_0 t/\gamma)^2+i\omega_0 t}, \tag{3}$$

which provides an excellent compromise between time and frequency resolution, because it is based on a Gaussian envelope (which guarantees the best possible time-frequency resolution).[9,10] Note that the variable γ controls the sharpness of the Gaussian envelope in the time domain.

Since the WT decomposes a signal into wavelet components (and not into sine components like the Fourier transform), there is not a direct map from wavelet scale, a, to frequency, ω. It is possible, however, to compute the WT of a sine, and then calculate the relationship between scale and frequency by determining the value a for which a scalogram reaches its maximum.[11] Finally, if broadband signals (such as laser-generated Lamb waves) are analyzed with the WT, the higher frequencies tend to have lower energies. As a result, it is advantageous to amplify high-frequency components by multiplying the WT with $(1/\sqrt{a})$[12]—this research uses the $1/\sqrt{a}$ scaled Gabor WT.

While the STFT is the Fourier transform of small, overlapping, windowed pieces of a time signal $s(t)$, the Wigner–Ville distribution (WVD) is the Fourier transform with respect to τ of $s(t+[\tau/2])s^*(t-[\tau/2])$ [where $s^*(t)$ is the complex conjugate of $s(t)$], or[8]

$$S_3(\omega,t)=\int_{-\infty}^{\infty}s\left(t+\frac{\tau}{2}\right)s^*\left(t-\frac{\tau}{2}\right)e^{-i\omega\tau}\mathrm{d}\tau. \tag{4}$$

As a result, the WVD is a measure of the signal's local time-frequency energy. An advantage of the WVD is that it can exactly localize sines or Dirac impulses; this is not the case for the spectrogram and the scalogram. Unfortunately, this property means that the WVD is real, but not necessarily positive [the only signal class that leads to a strictly positive WVD is $s(t)=(\alpha/\pi)^{1/4}e^{-(1/2)\alpha t^2+(1/2)i\beta t^2+i\omega_0 t}$], and that it suffers from signal interference. For example, the WVD can perfectly resolve a single chirp, but a signal consisting of two chirps will be decomposed into the two chirps themselves *plus an additional interference term*.

To avoid this interference, the WVD is often replaced by the smoothed WVD

$$S_4(t,f)=\int\int_{-\infty}^{\infty}G(t-t',f-f')S_3(2\pi f',t')\mathrm{d}t'\,\mathrm{d}f', \tag{5}$$

which filters the original WVD of Eq. (4) with a two-dimensional filter, G.[8] An unfortunate side effect of this smoothing is the introduction of time-frequency smearing which nullifies the WVD's property of exact localization of sines and impulses. This study uses the Gaussian filter

$$G(t,f)=\sqrt{\frac{1}{\alpha\beta}}e^{-(t^2/\alpha)-4\pi^2(f^2/\beta)}. \tag{6}$$

The value of the $\alpha\beta$ term in Eq. (6) controls both the positivity ($\alpha\beta\geqslant 1$ guarantees positivity) and signal localization of the resulting smoothed WVD. While the choice of $\alpha\beta \geqslant 1$ will guarantee positivity, the resulting distribution becomes a spectrogram and no longer possesses the WVD's advantages of signal localization.[13] As a result, it is critical to use a filter with $\alpha\beta<1$ in applications where superior signal localization (compared to the spectrogram) is desired.

The final TFR considered in this study is based on the empirical mode decomposition (EMD), that is used to generate a set of intrinsic mode functions (IMFs). Huang *et al.*[14,15] propose a method with which a complicated time-domain signal is decomposed into a finite number of IMFs that admit well-behaved Hilbert transforms. By using the Hilbert transform, the IMFs produce instantaneous frequencies *as functions of time*, that enable the identification of a signal's embedded structure (its modes). The resulting energy-time-frequency distribution is called the Hilbert spectrum, and is comparable to the spectrogram, scalogram, or WVD. This decomposition (the IMFs) is based on local properties of the signal itself, and not an artificial ''external'' function, so the instantaneous frequencies are (ideally) physically meaningful.

The decomposition of a signal, $s(t)$, into its IMFs is accomplished with a ''sifting'' process that uses the signal itself as the basis for the decomposition. Sifting empirically identifies the signal's intrinsic oscillatory modes by their characteristic time scales, and then decomposes the signal accordingly. The sifting process starts by first determining the maxima and minima of $s(t)$, and then connecting these maxima and minima with cubic splines (spline envelopes). In order to avoid (possible) erroneous behavior, such as wide swings of the spline envelopes at the signal's endpoints (both the right and left boundaries), ''artificial boundary conditions'' must be introduced. Huang *et al.*[14,15] propose the addition of characteristic waves at both ends of the signal. The sifting process (in brief) calculates the mean value, $m(t)$, of

a point on the maxima and minima spline envelopes and subtracts it from the original signal, $s(t)$, to obtain the first IMF candidate, or $h_1(t)=s(t)-m(t)$.[10,15] If h_1 is an IMF (h_1 is an IMF if the number of extrema and the number of zero crossings differs by at most 1, and if the mean value of h_1 defined by its spline envelope is zero), it is added to the list of calculated IMFs. If it is not, this step is repeated for k siftings—with $h_1, h_{12}, \ldots, h_{1k}$ leading (after k siftings) to the IMF, $h_{1k}(t)=h_{1(k-1)}(t)-m_{1k}(t)$. Once it meets the IMF definition, h_{1k} is subtracted from the original signal, producing the residue $r_1(t)=s(t)-h_{1k}(t)$. The complete process is then repeated with r_1 replacing the original signal to calculate the next IMF. The search for IMFs is stopped when a predetermined number of IMFs are calculated, or when r_n becomes monotonic—see the next section for a demonstration of the sifting process.

Having decomposed the signal $s(t)$ into n IMF components and a residue r_n, take the Hilbert transform of every IMF component, and add the (respective) Hilbert transform to every IMF to produce an analytic signal, $s_a(t)$. Next, determine the phase ϕ by

$$\phi(t)=\arctan\left(\frac{\mathcal{I}s_a(t)}{\Re s_a(t)}\right), \tag{7}$$

and phase unwrapping. The instantaneous (angular) frequency ω is computed by differentiating the phase ϕ, with respect to time. The Hilbert spectrum is then defined as the representation of the calculated amplitudes of the analytic signals of the IMFs, as a function of time and instantaneous frequency—a time-frequency representation of $s(t)$.

TFRs suffer from the Heisenberg uncertainty principle, making it impossible to *simultaneously* have perfect resolution in both time and frequency. The time-frequency resolution of a spectrogram depends only on the window size and type and is independent of frequency.[7,8] A wide window gives better frequency resolution, but worsens the time resolution, whereas a narrow window improves time resolution but worsens frequency resolution. In contrast, the scalogram tiles the time-frequency plane in an irregular fashion, resulting in a frequency-dependent time-frequency resolution.[9] The WT of small frequency values provides good frequency resolution, but the time resolution is bad. On the other hand, the WT of large frequency values provides poor frequency resolution, but the time resolution is good. The WVD automatically satisfies the uncertainty principle of a signal (as seen in the perfect localization of impulses and sines), but interference terms appear in multicomponent signals.[8,16] Smoothing the WVD with a Gaussian filter removes the interference terms, but changes the uncertainty of the resulting TFR—its uncertainty is quantified by the standard deviations (time and frequency) of the Gaussian filter, noting that the smoothed WVD becomes spectrogram-like with a Gaussian filter that guarantees positivity ($\alpha\beta \geqslant 1$). In contrast, the time-frequency accuracy of the Hilbert spectrum is dependent on the accuracy of the EMD—if the decomposition into IMFs does not capture the signal's real behavior, the resulting Hilbert spectrum will not give precise time-frequency results. Since the EMD is an empirical method, it is not possible to analyze an EMD's time-frequency resolution in as rigorous a fashion as for the spectrogram, scalogram or WVD.

It is possible to improve the time-frequency resolution of a TFR with the reassignment method;[17] the reassignment method improves the time-frequency resolution of a TFR by concentrating its energy at a center of gravity. Auger and Flandrin[18] provide a computationally efficient way to compute the reassigned values for the spectrogram and the scalogram, first proposed in Ref. 17. For example, calculating the reassigned spectrogram amounts to the calculation of the reassigned coordinates $(\hat{t},\hat{\omega})$ for each time-frequency pair (t, ω) in the original spectrogram, where

$$\hat{t}=t-\Re\left(\frac{S_{1_{\mathcal{T}h}}(x,t,\omega)\cdot\overline{S_{1_h}(x,t,\omega)}}{|S_{1_h}(x,t,\omega)|^2}\right), \tag{8}$$

and

$$\hat{\omega}=\omega-\mathcal{I}\left(\frac{S_{1_{\mathcal{D}h}}(x,t,\omega)\cdot\overline{S_{1_h}(x,t,\omega)}}{|S_{1_h}(x,t,\omega)|^2}\right). \tag{9}$$

S_{1_h}, $S_{1_{\mathcal{T}h}}$, and $S_{1_{\mathcal{D}h}}$ are the short-time Fourier transforms with window functions $h(t)$, $t\cdot h(t)$, and $[\mathrm{d}h(t)/\mathrm{d}t]$, respectively. The reassigned spectrogram is then given by

$$E_{1_{ra}}(\omega',t')=\frac{1}{2\pi}\int\int E_1(\omega,t)\,\delta(t'-\hat{t}(t,\omega)) \cdot\delta(\omega'-\hat{\omega}(t,\omega))\,\mathrm{d}t\,\mathrm{d}\omega, \tag{10}$$

where $\delta(t)$ is the Dirac impulse, and the integration is performed over the range of all t and ω. In summary, the reassigned spectrogram requires the calculation of three short-time Fourier transforms (with three different window functions). These transforms are then used to move each value of the spectrogram, $E_1(\omega,t)$ [at (t,ω)] to its reassigned coordinates, $(\hat{t},\hat{\omega})$, calculated with Eqs. (8) and (9). Finally, Eq. (10) is used to sum up values assigned to the same $(\hat{t},\hat{\omega})$ bin. Note that the reassignment method is not restricted to a specific TFR, but can be applied to any time-frequency shift invariant distribution of Cohen's class.[8] The Hilbert spectrum, however, does not meet this requirement.

III. APPLICATION OF TFRs TO LASER-GENERATED/DETECTED LAMB WAVES

Broad-bandwidth Lamb waves are generated with a Nd:YAG laser (4–6-ns pulse) and measured with a high-fidelity (resonance-free) laser interferometer over a wide frequency range (200 kHz to 10 MHz).[3] Figure 1 shows a (transient) time-domain signal with a propagation distance of 11 cm measured in a 0.93-mm aluminum plate. The Nd:YAG laser fires at $t=0$ and generates a Lamb wave at the source location. (Note that the electromagnetic discharge of the Nd:YAG's firing causes a spurious noise spike at $t=0$.) The signal in Fig. 1 is discretized with a sampling frequency of 100 MHz, low-pass filtered at 10 MHz, and represents an average of 100 Nd:YAG shots to increase the signal-to-noise ratio (SNR). It is important to note that the broad bandwidth, high fidelity, and high SNR (due to signal averaging) of this

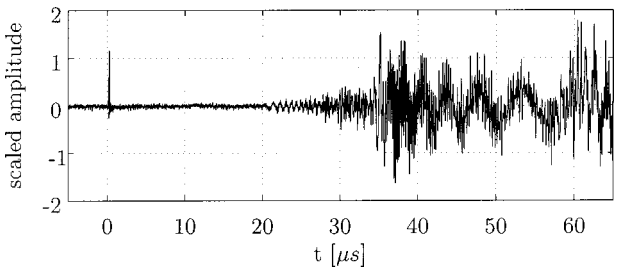

FIG. 1. Time-domain signal—multimode Lamb wave.

time-domain signal are crucial properties, making it an ideal signal to compare the effectiveness of the four candidate TFRs.

Assessment of the accuracy of the dispersion curves obtained with the candidate TFRs requires analytical results of the Rayleigh–Lamb frequency spectrum.[1] Solution of the Rayleigh–Lamb spectrum provides dispersion curves in the frequency-wave-number (f, k) domain, whereas a TFR maps a time-domain signal into the time-frequency domain. The group velocities for each of the different modes are determined by numerically differentiating f with respect to k to obtain the analytical dispersion curves in the time-frequency domain.[10]

Since Niethammer *et al.*[7] provide details on characterizing Lamb waves with the reassigned spectrogram, this paper briefly presents the results from this TFR, and only for comparison purposes. Figure 2 shows a contour plot of the square root of the reassigned spectrogram (384-point Hanning window) of the time-domain signal in Fig. 1, together with the analytically obtained dispersion curves as solid lines (all of the subsequent TFR plots include these analytical curves). The reassigned spectrogram provides a crisp definition of the individual modes, and these experimental modes are localized to the analytical curves. There is excellent definition of seven modes (s_0–s_2 and a_0–a_3) through a wide frequency range (up to 10 MHz). Note a general (and significant) advantage of TFRs in interpreting multimode Lamb waves—they enable the clear identification of the arrival time of the different modes (e.g., s_0 at 21 μs or a_0 at 35 μs). Finally, the

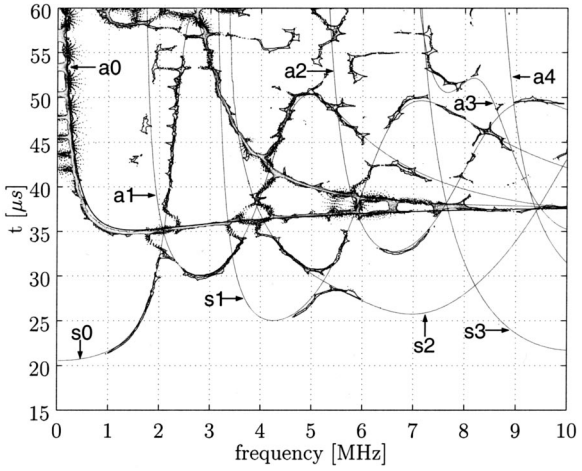

FIG. 2. Reassigned spectrogram of multimode Lamb wave, plus analytical solution (solid lines).

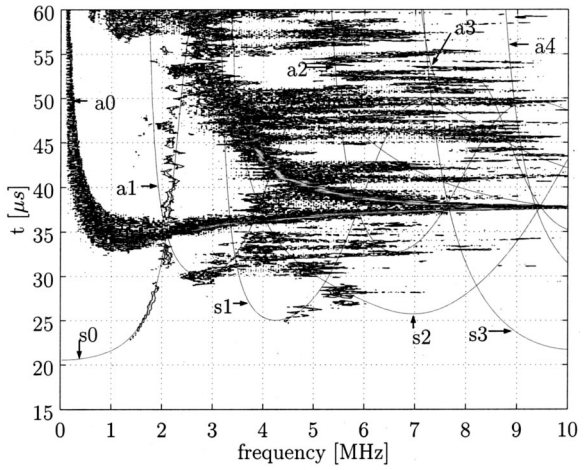

FIG. 3. Reassigned scalogram of multimode Lamb wave, plus analytical solution (solid lines).

broken lines above 50 μs are most likely caused by reflections from the plate's boundaries.

Figure 3 shows the square root of a reassigned scalogram of the same time-domain signal (Fig. 1) calculated with a Gabor wavelet. Although the time resolution at high frequencies is very good, there is not enough frequency resolution to separate the different modes at the high frequencies (e.g., above 2 MHz). The reassigned scalogram is effective in resolving the a_0 mode up to 10 MHz—an important feature for some applications. The WT has proven to be effective in many diverse applications (such as the detection of radar chirps), but a common theme in most of these applications is the need for good time resolution at high frequencies, and good frequency resolution at low frequencies. Figure 3 clearly shows that this attribute of the WT is not advantageous for resolving multiple, broadband Lamb modes. Note that an additional portion of this research[10] examines the Mexican-hat WT and shows its reassigned scalogram has even less resolution than the Gabor WT—the poor resolution in Fig. 3 is not due to improper selection of a mother wavelet, but instead is an inherent property of the WT.

The WVD and the smoothed WVD of the same time-domain signal (Fig. 1) are shown in Figs. 4 and 5, respectively. The results are stored in a 601×600 matrix, where columns correspond to a specific time and rows to a specific frequency (the frequency axis is equally spaced between 0 and 10 MHz, and the time axis has 0.1-μs discretization steps). The WVD of Fig. 4 is smoothed with a 21×21 Gaussian filter (which smoothes over a domain of 350 kHz $\times2.1$ μs) to create the smoothed WVD of Fig. 5. The selection of this particular filter size is based on ''visual'' comparisons, and note that it has $\alpha\beta<1$, so the resulting distribution is not positive (the negative values are set to zero in Fig. 5), but it provides good signal localization. Figure 4 shows that the WVD does a fairly good job in resolving the a_0 and the s_0 modes (they are both very localized) over a large frequency range—a_0 through the entire 10 MHz, and s_0 between 3 and 10 MHz. Unfortunately, all the other modes are obscured by interference terms and are not visible. The smoothed WVD of Fig. 5 provides a very good representation of the individual modes, with the s_0 and a_0 modes

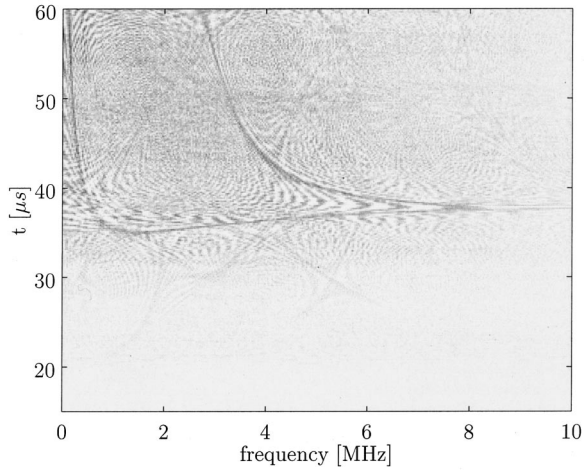

FIG. 4. Wigner–Ville distribution of multimode Lamb wave, plus analytical solution (solid lines).

clearly visible through the entire frequency bandwidth (to 10 MHz), the a_1 mode appears from 2 to 5 MHz, and traces of the s_1, s_2, and a_2 modes are evident. There is a general lack of time-frequency resolution (clarity) in the smoothed WVD. For example, it is difficult to positively identify the individual modes for frequencies above 5 MHz and times greater than 50 μs. The dispersion curves developed with the smoothed WVD (Fig. 5) render a mode resolution of about the same quality as the un-reassigned spectrogram.[7] It is important to note that it is possible to use a reassignment algorithm on the smoothed WVD[6,17] (the smoothed WVD of Fig. 5 has *not* been reassigned), but unlike the reassigned spectrogram and scalogram, the reassignment calculations for the smoothed WVD are computationally intensive (first requiring the smoothing procedure), difficult to implement, and time consuming (computationally).

The first step for the Hilbert spectrum is to decompose the time-domain signal of Fig. 1 signal into IMFs. Figure 6 shows the first seven IMFs, noting that the sifting process is stopped when a monotonic IMF (the 10th) occurs. Figure 6 shows that basically only the first 5 IMFs contain ''useful'' information, since IMFs above 5 are too low in frequency

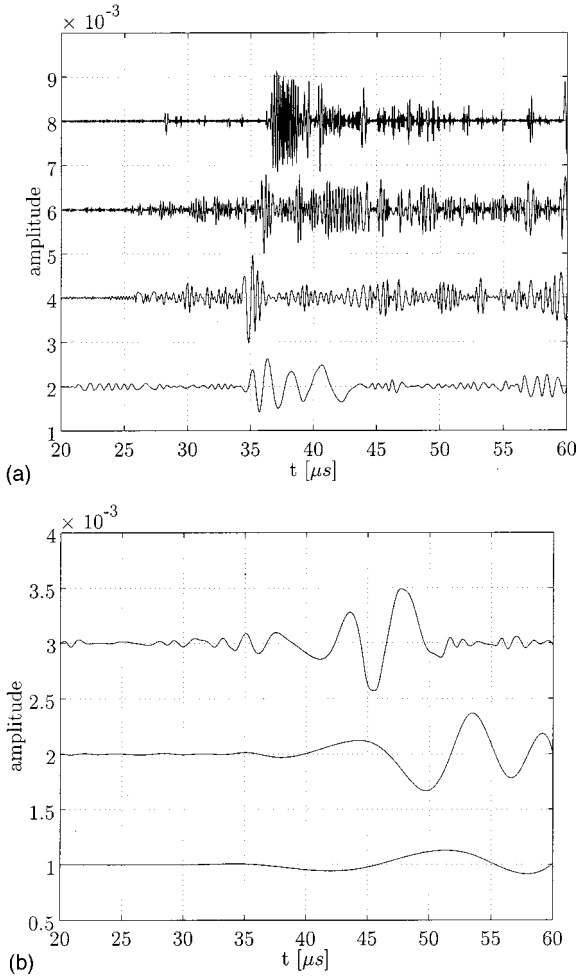

FIG. 6. (a) First four intrinsic mode functions (first to fourth from top to bottom) of multimode Lamb wave. (b) Fifth through seventh intrinsic mode functions (from top to bottom) of multimode Lamb wave.

(100 KHz or less) to be of importance for this application. Figure 7 shows a contour plot of the Hilbert spectrum computed from these IMFs, and it is far from being a ''clean'' representation of the dispersion curves of this signal. Only the a_0 mode is definitively present—a large number of points are clustered around the s_0 mode between 3 and 5 MHz, but

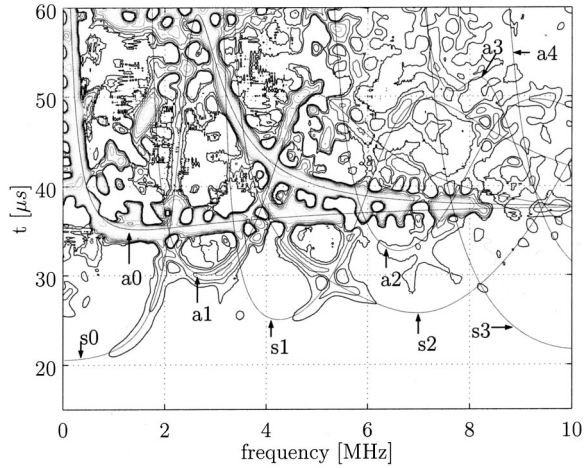

FIG. 5. Smoothed Wigner–Ville distribution of multimode Lamb wave, plus analytical solution (solid lines).

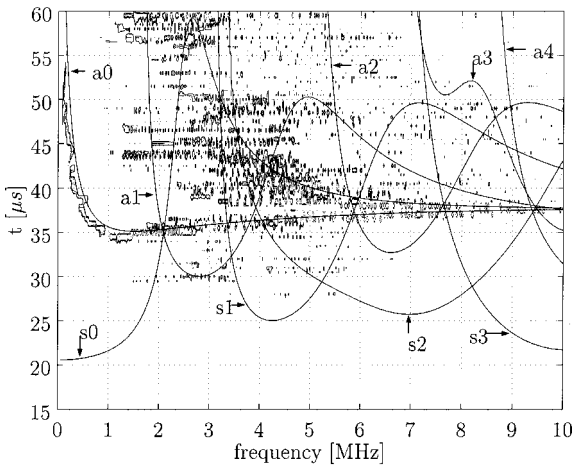

FIG. 7. Hilbert spectrum of multimode Lamb wave, plus analytical solution (solid lines).

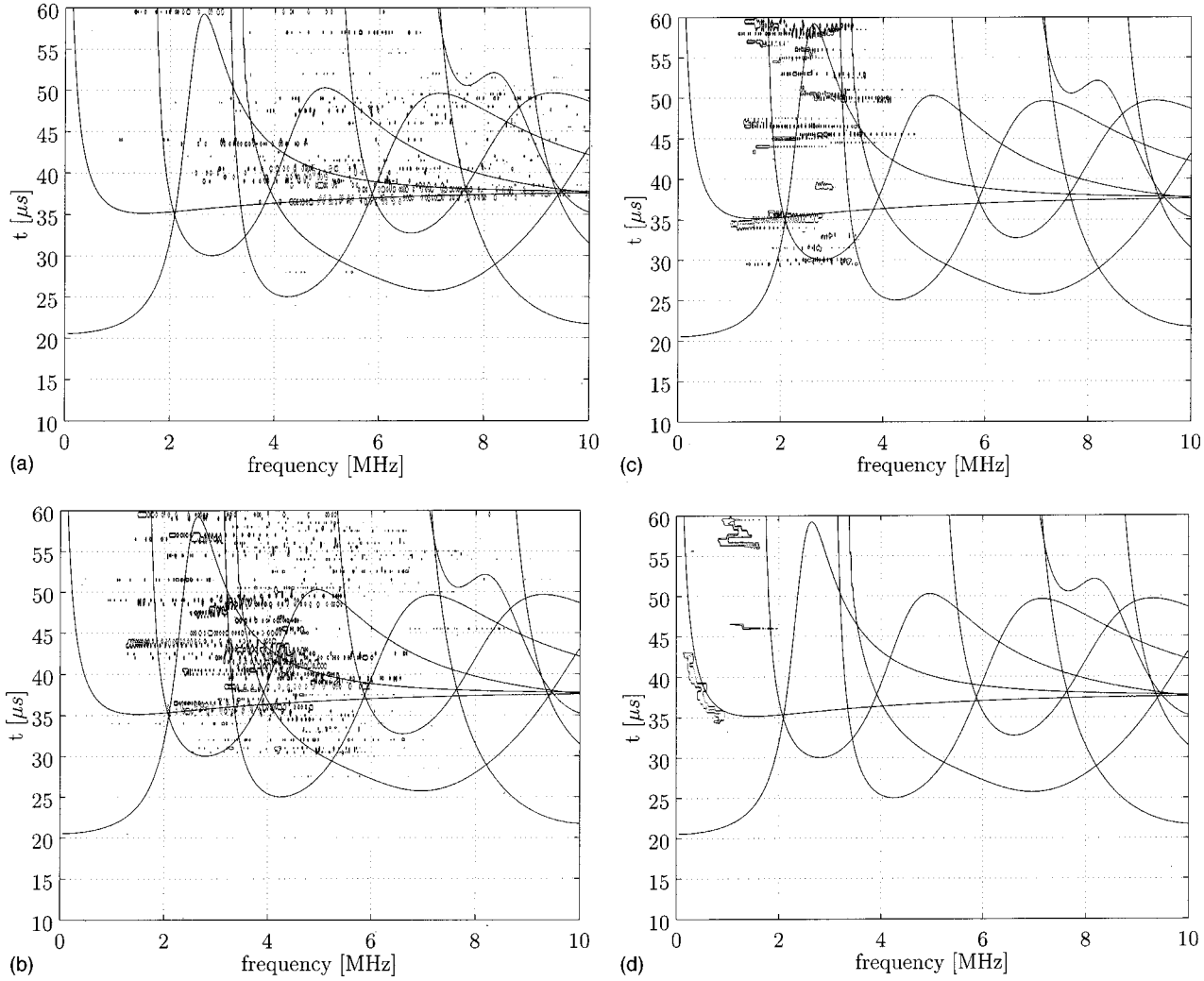

FIG. 8. (a) Hilbert spectra of first IMF, plus analytical solution (solid lines). (b) Hilbert spectra of second IMF, plus analytical solution (solid lines). (c) Hilbert spectra of third IMF, plus analytical solution (solid lines). (d) Hilbert spectra of fourth IMF, plus analytical solution (solid lines).

this mode is not clearly defined. In order to interpret the Hilbert spectrum of Fig. 7, Fig. 8 shows the instantaneous frequencies of the first four IMFs. By analyzing the Hilbert spectra of each IMF, it is possible to determine exactly which IMFs contribute to exactly which features in the Hilbert spectrum. For example, IMF 1 contains most of the a_0 and the s_0 modes between 4 and 10 MHz [Fig. 8(a)], but fails to localize its energy exactly on either mode—the first IMF scatters its energy around both a_0 and s_0. Also note the high level of noise present in IMF 1. IMF 2 contributes to the frequency band from 2 to 6 MHz [Fig. 8(b)]; except for a very small part of the a_0 mode at approximately 3 MHz, there is not an obvious correlation between the analytical modes and the resulting Hilbert spectrum. IMF 3 is quite effective in representing the a_0 mode from 1 to 3 MHz [Fig. 8(c)], but it fails to represent the other modes in the same frequency range. IMF 4 constitutes the a_0 mode from 35 to 45 μs [Fig. 8(d)]. It appears that each IMF specializes in a certain frequency range for these laser-generated/detected Lamb waves. This approach works fine for frequency ranges where there are only a few modes present, but it clearly fails for frequency ranges that contain multiple modes. This failure for multiple modes occurs because there is only one instantaneous frequency for an IMF for any time *t*. As a result, the EMD and Hilbert spectrum cannot resolve the multimode dispersion curves for this plate.

An inherent problem associated with all window-based TFRs (and thus their respective reassigned representations) is the ''ladder-like'' effect that occurs when the distance between two mode lines is less than the uncertainty of their representations. These mode lines will then interfere with each other, resulting in a smeared representation—this behavior is particularly evident when mode lines intersect each other (e.g., the intersection of the s_0, a_0, and a_1 modes at 2 MHz in Figs. 2–5). Image-processing methodologies that take the specific mode structure into account are a possible remedy for this smearing. Note that the comparison between these TFRs is generic enough to be extended to any plate thickness and material. As an example of the general nature of these results, the reassigned spectrogram has been used to successfully resolve the dispersion relationships for multimode circumferential waves in a cylinder.[10]

IV. CONCLUSION

This paper establishes the effectiveness of four candidate TFRs to analyze broadband, multimode ultrasonic

waves. All TFRs are not equally suited to represent every signal type, so a vital contribution of this study is the identification of which TFRs are most effective for analyzing multimode Lamb waves, and why. Overall, this paper illustrates the effectiveness of using TFRs to quantitatively resolve changes in the frequency content of these nonstationary signals, as a function of time. Another strength of TFRs demonstrated in this study is their ability to facilitate the identification of the arrival times of the different modes in a multimode signal.

This research shows that the reassigned spectrogram is extremely effective in localizing multiple, closely spaced Lamb modes in both time and frequency. The reassigned scalogram can only accurately resolve a single mode (the a_0) in this multimode Lamb wave; this deficiency is attributed to the method's insufficient frequency resolution for high frequencies. The WVD is ineffective in this application, while the smoothed WVD provides a very good representation of the individual Lamb modes, while showing a general lack of time-frequency clarity (note that with more smoothing, the WVD becomes similar to a spectrogram). Note that the time-frequency resolution of the smoothed WVD can be improved with a reassignment algorithm (like the reassignment of the spectrogram and scalogram). Unfortunately, the reassignment calculations for the smoothed WVD are intensive (first requiring the smoothing procedure), difficult to implement, and computationally time consuming. As a result, the reassigned spectrogram appears to be a better choice to characterize these multimode Lamb waves. Even though the EMD combined with the Hilbert transform is based on local properties of the signal itself, this study shows that this Hilbert spectrum technique is not capable of extracting the Rayleigh–Lamb frequency spectrum between 200 kHz and 10 MHz, from a laser-generated/detected time-domain signal. The Hilbert spectrum fails because of the plate's intricate mode structure, with multiple modes occupying the same frequency band, and intersecting each other in time and frequency.

ACKNOWLEDGMENTS

This work is supported by the Office of Naval Research M-URI Program ''Integrated Diagnostics'' (Contract Number: N00014-95-1-0539). The Deutscher Akademischer Austausch Dienst (DAAD) provided partial support to Marc Niethammer. The authors thank NASA Goddard for providing them with the EMD/Hilbert Spectrum software and Christoph Eisenhardt for his contributions in making the experimental measurements.

[1] R. D. Mindlin, ''Waves and vibrations in isotropic elastic plates,'' in *Structural Mechanics*, edited by J. N. Goodier and N. J. Hoff (Pergamon, New York, 1960).

[2] D. Alleyne and P. Cawley, ''A two-dimensional Fourier transform method for measurement of propagating multimode signals,'' J. Acoust. Soc. Am. **89**, 1159–1168 (1991).

[3] C. Eisenhardt, L. J. Jacobs, and J. Qu, ''Application of laser ultrasonics to develop dispersion curves for elastic plates,'' J. Appl. Mech. **66**, 1043–1045 (1999).

[4] W. H. Prosser, M. D. Seale, and B. T. Smith, ''Time-frequency analysis of the dispersion of Lamb modes,'' J. Acoust. Soc. Am. **105**, 2669–2676 (1999).

[5] Y. Hayashi, S. Ogawa, H. Cho, and M. Takemoto, ''Noncontact estimation of thickness and elastic properties of metallic foils by wavelet transform of laser-generated Lamb waves,'' Nondestr. Test. Eval. **32**, 21–27 (1999).

[6] S. Holland, T. Kosel, R. Weaver, and W. Sachse, ''Determination of plate source, detector separation from one signal,'' Ultrasonics **38**, 620–623 (2000).

[7] M. Niethammer, L. J. Jacobs, J. Qu, and J. Jarzynski, ''Time-frequency representation of Lamb waves using the reassigned spectrogram,'' J. Acoust. Soc. Am. **107**, L19–L24 (2000).

[8] L. Cohen, *Time-Frequency Analysis* (Prentice-Hall, Englewood Cliffs, NJ, 1995).

[9] S. Mallat, A *Wavelet Tour of Signal Processing* (Academic, New York, 1998).

[10] M. Niethammer, ''Application of Time-Frequency Representations to Characterize Ultrasonic Signals,'' M.S. thesis, Georgia Institute of Technology, Atlanta, 1999.

[11] S. D. Meyers, B. G. Kelly, and J. J. OBrien, ''An introduction to wavelet analysis in oceanography and meterology: With application to the dispersion of Yanai waves,'' Mon. Weather Rev. **121**, 2858–2866 (1993).

[12] D. Casasent and R. Shenoy, ''New Gabor wavelets with shift-invariance for improved time-frequency analysis and signal detection,'' in Proc. SPIE **2762**, Wavelet Applications III, edited by H. Szu, 244–255 (1996).

[13] L. Cohen, ''A Primer on Time-Frequency Analysis,'' in Time-Frequency Signal Analysis, edited by B. Boashash (Longman Chesire, 1992), pp. 3–42.

[14] N. E. Huang, Z. Shen, and S. R. Long, ''A new view of nonlinear water waves: The Hilbert spectrum,'' Annu. Rev. Fluid Mech. **31**, 417–457 (1999).

[15] N. E. Huang, Z. Shen, S. R. Long, M. C. Wu, H. H. Shih, Q. Zheng, N.-C. Yen, C. C. Tung, and H. H. Liu, ''The empirical mode decomposition and the Hilbert spectrum for nonlinear and non-stationary time series analysis,'' Proc. R. Soc. London, Ser. A **454**, 903–995 (1998).

[16] L. Cohen, ''Time-frequency distributions—A review,'' Proc. IEEE **77**, 941–981 (1989).

[17] K. Kodera, R. Gendrin, and C. de Villedary, ''Analysis of time-varying signals with small BT values,'' IEEE Trans. Acoust., Speech, Signal Process. **26**, 64–76 (1978).

[18] F. Auger and P. Flandrin, ''Improving the readability of time-frequency and time-scale representations by the reassignment method,'' IEEE Trans. Signal Process. **43**, 1068–1089 (1995).